Available online at www.sciencedirect.com

SciVerse ScienceDirect

Ceramics International 39 (2013) 367–375

CERAMICS INTERNATIONAL

www.elsevier.com/locate/ceramint

Thermal shock behavior of nano-sized ZrN particulate reinforced AlON composites

N. Zhang[a,*], X.J. Zhao[a,b], H.Q. Ru[b], X.Y. Wang[a,b], D.L. Chen[c]

[a]Key Laboratory of Advanced Materials Manufacturing Technology of Liaoning Province, Shenyang University, Shenyang, Liaoning 110044, China
[b]Department of Materials Science and Engineering, School of Materials and Metallurgy, Northeastern University, Shenyang, Liaoning 110004, China
[c]Department of Mechanical and Industrial Engineering, Ryerson University, Toronto, Ontario, Canada M5B 2K3

Received 23 April 2012; received in revised form 12 June 2012; accepted 13 June 2012
Available online 17 June 2012

Abstract

Aluminum oxynitride (AlON) has been considered as a potential ceramic material for high-performance structural and advanced refractory applications owing to its excellent stability and mechanical properties such as high rigidity and good chemical stability. Thermal shock resistance is a major concern and an important performance index of refractories and high-temperature ceramics. While zirconium nitride (ZrN) particles have been proven to improve mechanical properties of AlON ceramic, the thermal shock behavior has not been evaluated yet. The aim of this investigation was to identify the thermal shock resistance and underlying mechanisms of hot-pressed 2.7% ZrN–AlON composites by a water-quenching technique over a temperature range between 225 °C and 275 °C. The residual strength and Young's modulus after thermal shock decreased with increasing temperature range and thermal shock times due to large temperature gradients and thermal stresses caused by abrupt water-quenching. The presence of nano-sized ZrN particles exhibited a positive effect on the improvement of both residual strength and critical temperature difference of AlON ceramic due to the toughening effects, the higher thermal conductivity of ZrN, the refined grain size and the reduction of porosity. Different toughening mechanisms including crack deflection, crack bridging and crack branching were observed during thermal shock experiments, thus effectively enhancing the crack initiation and propagation resistance and leading to a considerable improvement in thermal shock resistance in the ZrN–AlON composites.

Keywords: AlON; ZrN; Thermal shock; Ceramic

1. Introduction

Ceramics are brittle and fail catastrophically when subjected to steady state, non-steady state mechanical or thermomechanical stresses. In many applications ceramics and refractory materials are exposed to thermomechanical stresses because of the thermal shock/transient thermal conditions (a sudden change in temperature), for example in a high temperature furnace or in a gas turbine engine [1]. Under these thermal transient conditions ceramics are susceptible to catastrophic failure because of their brittleness, relatively low thermal conductivity, and high Young's modulus of elasticity [2]. Thermal shock resistance is an important feature of refractories and ultra-high temperature ceramics, which frequently determines a possibility of their applications such as aerospace and astronautic industries [3–5].

Owing to the excellent chemical and mechanical properties such as high rigidity, good chemical stability, superior corrosion and wear resistance, spinel aluminum oxynitride (AlON) as a solid solution of Al_2O_3 and AlN [2,6] has been considered as a promising candidate ceramic material to be used in high-performance structural and advanced refractory applications [7,8]. Some studies [9,10] have involved the thermal shock behaviors of AlON ceramics. Corbin [9] reported that the critical temperature difference of AlON was only about 175 ± 5 °C. Zhao et al. [10] reported that the critical temperature differences for AlON ceramic and SiC–AlON composites were about 200 °C and 225 °C, respectively. Although AlON ceramics have many advantages, their

*Corresponding author. Tel./fax: +86 24 62266946.
E-mail address: zhangning5832@163.com (N. Zhang).

0272-8842/$36.00
http://dx.doi.org/10.1016/j.ceramint.2012.06.036

intrinsic characteristics such as low fracture toughness (premature failure due to brittle fracture) and low toughness-induced poor thermal shock resistance would be still obstacles for this type of material to be further used widely, especially in some severe environments.

Zirconium nitride (ZrN) is an attractive candidate for high-temperature applications because of its excellent chemical and mechanical properties such as high chemical and thermal stability, high hardness, abrasive resistance and good electrical conductivity [11,12]. It has a number of technological applications, such as refractory material [13], hard coating for cutting tools [14] and Josephson junctions in electronics [15]. The ZrN particles were proven to effectively improve the mechanical properties of AlON ceramic. However, to the authors' knowledge, there is no report in the open literature regarding the thermal shock behavior of ZrN–AlON composites. The questions remain if and to what extent the nano-sized ZrN particles can improve the thermal shock resistance of AlON ceramic. The aim of the present study was, therefore, to evaluate and analyze the thermal shock behavior of ZrN–AlON composites, with special attention to the influence of nano-sized ZrN particles on the thermal shock resistance of ZrN–AlON composites.

2. Materials and methods

2.1. Preparation of samples

In the present study, the commercial m-ZrO_2 (40–100 nm, Nanjing Emperor Nano Material Co., Ltd., China, 99%) powders and AlON powders prepared using Al_2O_3 (40–100 nm, Nanjing Emperor Nano Material Co., Ltd., China, 99.5%) and AlN (30–100 nm, Shenzhen Honesty Nano-Tech Co., Ltd., China, 99%) were used as raw materials. Due to the superior mechanical properties of ZrN–AlON ceramic composites, 6 wt% nano-sized ZrO_2 particles were added into the AlON mixture in the present work. The thoroughly mixed powders were attrition milled for 24 h using ethanol as a milling medium, and then dried at 80 °C. The dry mixed ZrO_2–AlON powders were crushed using a mortar and then sieved through a 180 μm mesh. The mixed powders were put in a graphite dye and sintered at 1850 °C under a pressure of 25 MPa for 40 min in nitrogen atmosphere at a heating rate of 10 °C/min below 1400 °C and then 5 °C/min up to the selected sintering temperature. Finally the sintered ZrN–AlON composites were furnace-cooled down to room temperature.

2.2. Characterization of materials

The flexural strength was measured using a three-point bending (TPB) system that was performed with 1 kN load cell and using a TPB stage with a span of 20 mm attached to a computerized Instron 8801 fatigue testing system. In the TPB tests the cross-head speed was set at a rate of 0.2 mm/min in accordance with ASTM C1161. The values of flexural strength σ and Young's modulus E were calculated according to the following equations [16]:

$$\sigma = 3FL/(2bh^2), \tag{1}$$

$$E = kL^3/(4bh^3), \tag{2}$$

where F is the load at failure (N), L is the span (mm), b is the sample width (mm), h is the thickness (mm) and k is the slope (dF/dv) in the load–deflection curve. To evaluate the slope k more accurately, a load range of 5N to the load at failure was used in all the TPB tests.

Thin disks (3 mm Ø) of sintered ZrN–AlON composites were subsequently prepared by ultrasonic cutting, dimpling, polishing, and ion milling. Microcharacterization was performed using transmission electron microscopy (TEM) and electron diffraction (ED). The microstructures including the powder size, the fracture surface and crack propagation were examined using a scanning electron microscope (SEM). To achieve a better resolution on the SEM images, the specimens were sputter-coated with a thin film of gold. The phase and crystallinity were analyzed via X-ray diffraction (XRD) using CuK_α radiation at 45 kV and 40 mA. The diffraction angle (2θ) at which the X-rays hit the sample varied from 10° to 90° with a step size of 0.05° and 1 s in each step.

2.3. Thermal shock experiments

Thermal shock experiments were performed in an electric muffle furnace and air atmosphere via water-quenching. The thermal shock test samples, with a dimension of 25 mm × 2 mm × 2 mm, were ground and polished to a surface finish using 1 μm diamond paste. Water was used as the quench medium and kept at a constant temperature of 25 °C. In each thermal shock test, a specimen was heated to temperatures of 225 °C, 250 °C and 275 °C and kept in the furnace for 20 min, and then quenched into the water bath for 30 s to ensure temperature uniformity. The subsequent heating cycle identical to the previous one was carried out immediately after quenching and drying of samples. The residual strength was measured at room temperature using a TPB test set-up attached to a computerized Instron 8801 fatigue testing system. Because the residual strength of the specimens after 1 time quenching was observed to be close to the original strength, 3 times quenching was selected in the present experiments of residual strength as a function of thermal shock temperature for ZrN–AlON composites. Also, three thermal shock samples were prepared and tested in each condition, and the average values were reported. The microstructural features of the ceramic materials after thermal shock tests were observed using SEM.

3. Results

3.1. Microstructure of raw powders

Fig. 1 shows the SEM micrographs of the prepared AlON powders and ZrO_2 powders. It is seen from Fig. 1(a) that the

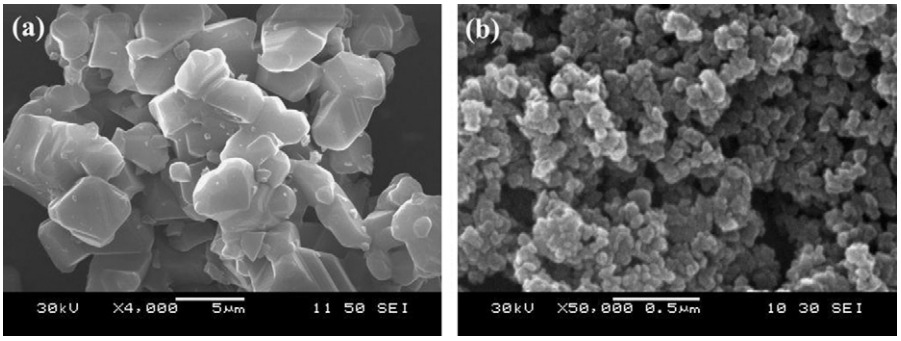

Fig. 1. SEM micrographs of raw powders for the (a) AlON powders and (b) nano-sized ZrO_2 powders.

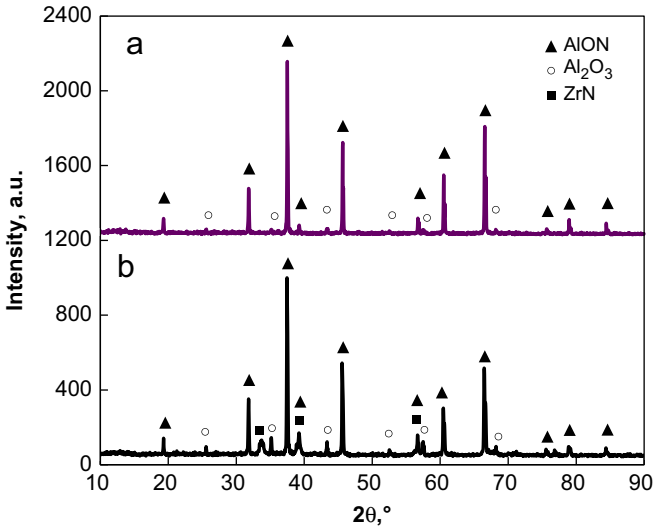

Fig. 2. XRD patterns of (a) pure AlON and (b) 2.7% ZrN–AlON composites sintered in a nitrogen atmosphere at 1850 °C.

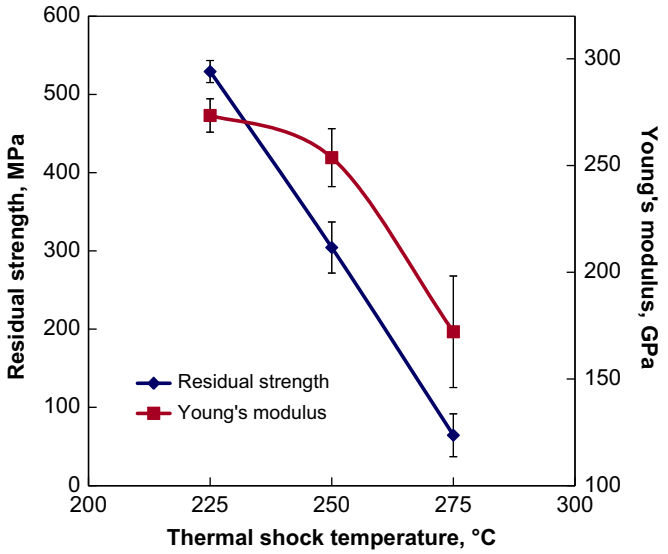

Fig. 3. Residual flexural strength and Young's modulus of 2.7% ZrN–AlON composites as a function of quenching temperature after 3 times thermal shock tests.

AlON powders had an average size of about 4 μm. Besides, the spinel-type structure of prepared AlON powders was similar to that reported in [9,17]. Fig. 1(b) shows that most ZrO_2 particles were nano-sized (< 100 nm), but there also appeared a conglomeration because it was rather difficult to disperse nano-sized particles on a copper plate even after ultrasonic vibration for SEM imaging.

3.2. X-ray diffraction analysis

Fig. 2 shows the XRD patterns of pure AlON and AlON composites with 6 wt% ZrO_2 addition. It is seen that γ-AlON ($Al_{2.81}O_{3.56}N_{0.44}$) has been detected in both pure AlON and AlON composites, which is similar to that reported in [6,17]. The obtained AlON exhibited a typical XRD pattern of AlON without decomposition (i.e., no other by-products present), as seen in Fig. 2(a). It is interesting that the ZrN phase was observed and no ZrO_2 phase was present after hot press sintering at 1850 °C. Furthermore, in comparison with pure AlON (Fig. 2(a)), a slight increase in the content of Al_2O_3 phase was observed in the ZrN–AlON composites (Fig. 2(b)). It was mainly attributed to the reaction of AlON matrix with added ZrO_2 particles, which formed as ZrN and Al_2O_3. If the 6 wt% ZrO_2 was assumed to change into ZrN completely, the volume percent of ZrN phase in the ZrN–AlON composites was estimated to be about 2.7% in the present work. Also, the spectra as shown in Fig. 2(b) revealed that the 2.7% ZrN–AlON composites consisted mainly of AlON, ZrN and a small amount of Al_2O_3, and no other phase could be identified in the pattern.

3.3. Change in mechanical properties during thermal shock tests

Fig. 3 shows the residual strength and Young's modulus of 2.7% ZrN–AlON composites as a function of thermal shock temperature after three thermal shock cycles. It is seen that the residual strength and Young's modulus of 2.7% ZrN–AlON composites decreased with increasing thermal shock temperature. Similar results have been reported for the mullite ceramic [18], ZrC matrix ceramics [19] and ZnS–SiO_2 composites [20]. The detailed

explanation will be presented in the discussion section. As shown in Fig. 3, when the thermal shock temperature was 225 °C, the residual strength of ZrN–AlON composites was 529 MPa that was basically close to the flexural strength of 556 MPa obtained at room temperature within the experimental scatter. However, with further increasing thermal shock temperature, the residual strength decreased drastically. When the thermal shock temperature was 250 °C and 275 °C, the residual strength was about 304 MPa and 64 MPa, respectively. Since the residual strength of 2.7% ZrN–AlON composites after 3 times of thermal shock tests at 250 °C decreased to about half of the original flexural strength, indicating this temperature being a critical thermal shock temperature, the subsequent tests involving the influence of quenching time on the residual strength of 2.7% ZrN–AlON composites were carried out at 250 °C. While Young's modulus decreased with increasing thermal shock temperature as well, the decrease was not so pronounced in comparison with that of the residual flexural strength, because Young's modulus represents a measure of the resistance to the separation of adjacent ions (or atoms) or the interatomic bonding forces, with a strong effect of defects (pores, cracks) in the material.

Fig. 4 shows the variation of residual flexural strength and Young's modulus of 2.7% ZrN–AlON composites with the number of quenchings. It is obviously seen from Fig. 4 that both residual strength and Young's modulus decreased with increasing number of repeated thermal shock tests in ZrN–AlON composites. However, after 5 times of repeated thermal shock tests, both the residual strength and Young's modulus of the ZrN–AlON composites seemed to be exhausted. As seen from Fig. 4, after 5 times thermal shock tests, only about 13% of the original flexural strength was indeed retained for ZrN–AlON composites. The above results indicated that the thermal shock had a strong effect on the ZrN–AlON composites.

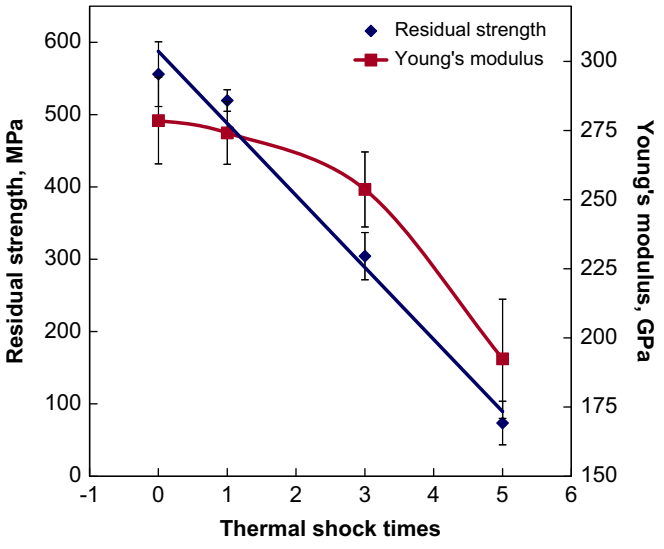

Fig. 4. Residual flexural strength and Young's modulus of 2.7% ZrN–AlON composites as a function of the number of thermal shock tests carried out at 250 °C.

3.4. Change in microstructures during thermal shock tests

Fig. 5 shows the typical TEM micrographs of ZrN–AlON composites before thermal shock experiments and ED patterns of AlON and ZrN phases. From Fig. 5(a), the AlON matrix grain with a size of about 4 μm can be clearly seen. As shown in Fig. 5(a) and (b), the ZrN particles are indicated by arrows homogeneously distributed in the AlON matrix, mainly located at grain boundaries or triple junctions of AlON grains. It is interesting to note that most ZrN particles transformed from ZrO_2 still remained to be nano-sized after sintering at 1850 °C. In comparison with pure AlON with a grain size of about 5 μm as reported in [10], it can be seen that the presence of ZrN particles effectively restricted the growth of grains, leading to a refined AlON matrix grain size. This was attributed to the pinning effect (Zener pinning pressure) of the nano-sized ZrN particles positioned at grain boundaries or triple junctions of AlON, which was one of the well-recognized processes that reduced the driving force for grain growth [21]. The refined grain would play an important role in the improvement of mechanical properties and thermal shock resistance of ZrN–AlON composites. A detailed explanation will be given in the next section. The different phases of AlON and ZrN were also identified by ED analysis as shown in Fig. 5(c) and (d). They are in agreement with the composition of the phases found by XRD analysis in Fig. 2. $Al_{2.81}O_{3.56}N_{0.44}$ (cubic structure and Fd-3m space group) was observed in ZrN–AlON composites, and the zone axes along [110] are presented in Fig. 5(c). ZrN (cubic structure and Fm-3m space group) was found in the ZrN–AlON composites and its ED pattern along [211] can be seen in Fig. 5(d).

Fig. 6 shows the SEM images of overall fracture surfaces of TPB specimen of 2.7% ZrN–AlON composites after different numbers of repeated quenchings from 250 °C. When no thermal shock was done, or it was done for 1 time at 250 °C for ZrN–AlON composites, the crack initiation occurred from the bottom surface of the TPB samples, as indicated by the arrows in Fig. 6(a) and (b), where the tensile stress reached a maximum. Besides, no obvious crack caused by the 1 time thermal shock can be seen in Fig. 6(b), thus the residual strength was close to the original strength that also corresponded well to the measured results as shown in Fig. 4. With increasing number of thermal shock tests, the pre-existing crack induced by the earlier thermal shock exhibited obvious propagation, as indicated by the different facets in Fig. 6(c) and (d) where the fracture surfaces experienced multiple repeated thermal shock tests were different from the relative smooth surface without thermal shock (Fig. 6(a)). The different facets that appeared on the fracture surface experiencing multiple quenchings indeed indicated the occurrence of crack branching or deflection. This was attributed to the fact that in each quenching the sample got into water

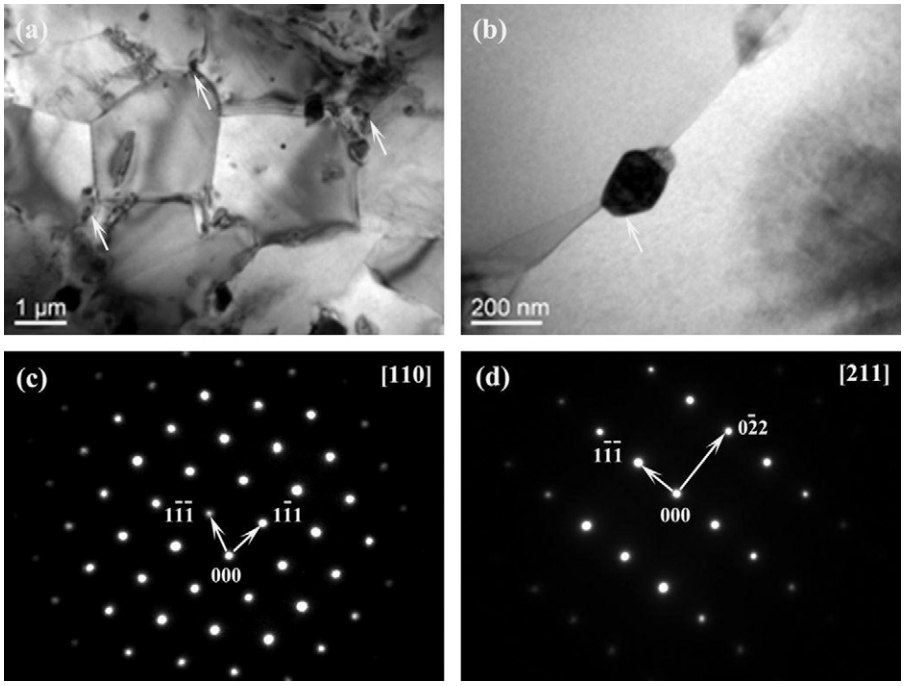

Fig. 5. Typical bright field TEM micrographs of 2.7% ZrN–AlON composites: (a) low magnification; (b) high magnification; and ED patterns of (c) along [110] according to the AlON phase; (d) along the [211] according to the ZrN phase in the ZrN–AlON composites.

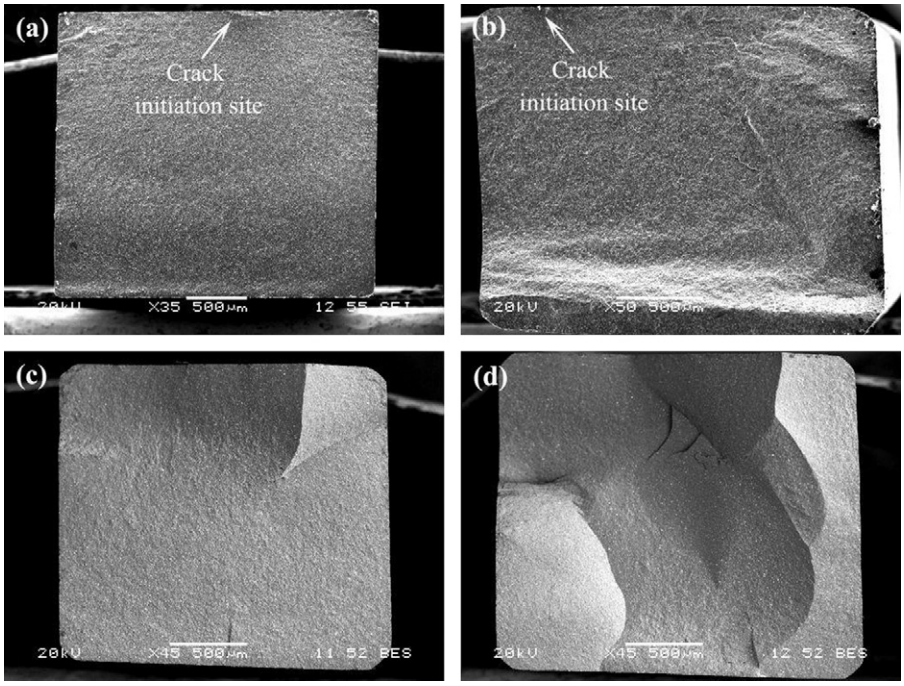

Fig. 6. SEM images of full TPB specimen fracture surfaces of 2.7% ZrN–AlON composites after (a) 0 time; (b) 1 time; (c) 3 times; and (d) 5 times of quenching from 250 °C.

randomly or at different angles, causing different temperature gradients and internal residual stresses and thus changing the cracking direction. As a consequence, the formation of a thermal shock-induced crack and the subsequent crack propagation together with the formation of new potential cracks led to a remarkable decrease in the residual strength and Young's modulus (Fig. 4) with increasing number of repeated thermal shock tests.

Fig. 7 shows the SEM micrographs from the fracture surface of 2.7% ZrN–AlON composites after thermal shock tests from a temperature of 250 °C. It is seen that the fracture surface of ZrN–AlON specimen after thermal

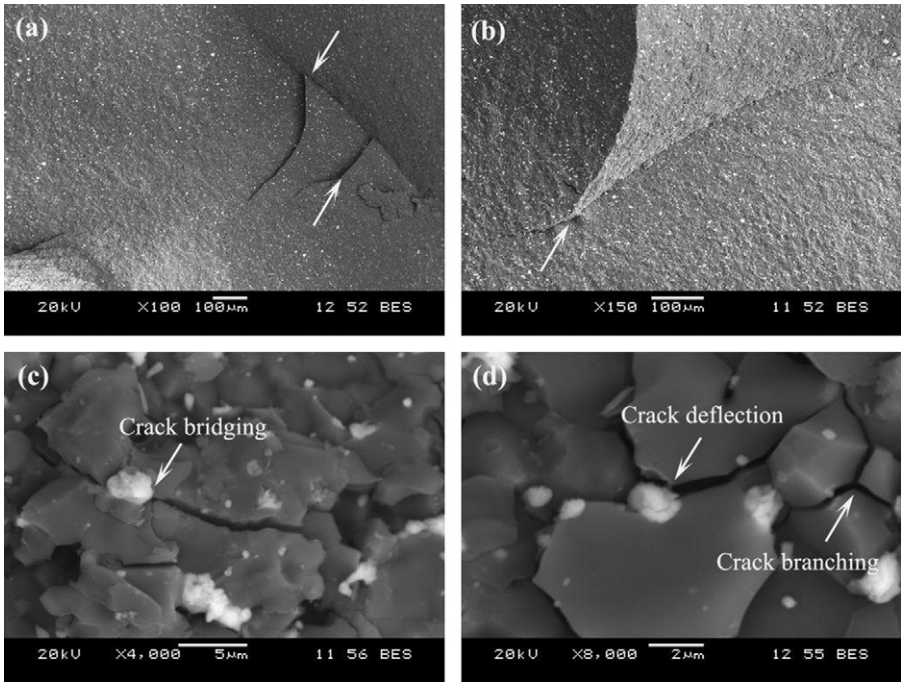

Fig. 7. SEM micrographs of fracture surfaces of ZrN–AlON composites after thermal shock from a temperature of 250 °C.

shock tests basically exhibited cleavage fracture features. With the presence of ZrN particles, crack deflection, bridging and branching tended to occur frequently, as indicated by the arrows in Fig. 7. This was due to the pinning role of the nano-sized ZrN particles that located at grain boundaries or triple junctions of AlON grains as shown in Fig. 5 and the different coefficients of thermal expansion between ZrN and AlON. It indicated that the presence of ZrN particles played an important role to improve the thermal shock resistance of AlON ceramic. Details will be present in the next section.

4. Discussion

It should be initially noted that the critical thermal shock temperature of AlON was about 200 °C that was reported in our recent publication [10]. Then, the ZrN–AlON composites had an original flexural strength of 556 MPa, fracture toughness of 2.46 MPa $m^{1/2}$ and Young's modulus of 278 GPa in the present study. Additionally, the materials of hot-pressed ZrN–AlON composites reached a relative density of 99.5% according to the Archimedes measurement [17].

During a sudden temperature change of a body, there occurred transient temperature distribution which induced thermal stresses called thermal shock [18]. Quenching-strength test is a common method used to evaluate the thermal shock resistance of ceramic materials because the strength degradation reflects thermal damage of a material [22]. When a sudden heating or cooling happens on ZrN–AlON composites material, thermal shock loading condition would be created to generate different thermal stresses [23,24]. Han and Wang [25] reported that the thermal shock resistance of ceramic material is very sensitive to their temperature-dependent material properties. As shown in Fig. 3, after thermal shocking below a temperature of 225 °C, the elastic strain energy caused by thermal stresses was relatively low, and did not provide for the driving force required for the nucleation and propagation of cracks. Thus no crack or other forms of damage in the specimen interior were observed, leading to no change in both the residual strength and Young's modulus (Fig. 3). However, when the ZrN–AlON samples were subjected to thermal shock at or over 250 °C, due to the increase of temperature gradients and resulting elastic strain energy, cracks were produced to release the elastic strain energy stored, which was transformed into the effective surface energy, and then the ceramic samples became stress-free. The effective surface energy, which increased via crack propagation, was accomplished by generation of newly formed crack surfaces [19], as also shown in Figs. 6 and 7. The observed results also correspond well with those of Buchheit et al. [26], who reported that the thermal shock behavior typically exhibits three stages in most shock testing: in the first stage, quenched specimens show no strength degradation compared with unquenched materials because the stresses generated during quenching are lower than those required for crack initiation or for growth of cracks already present in the specimen; in the second stage, the specimens show a drop in flexural strength, either immediate or prolonged over a large temperature range; when the retained strength levels off, in the third stage, long cracks present in the specimens experience subcritical crack growth.

Based on the experiments of water-quenching into 25 °C, the critical thermal shock test temperature of ZrN–AlON ceramic was observed to be about 250 °C. Thus, the critical temperature difference of ZrN–AlON composites became 225 °C. As mentioned before, the critical temperature difference of pure AlON was about 200 °C using the same investigated method [10]. Therefore, it illustrated clearly that the nano-sized ZrN particulate reinforced AlON composites had a better thermal shock resistance than pure AlON ceramic.

According to the damage type of ceramic materials after being subjected to thermal shock, the classic theory on the thermal shock resistance of brittle ceramics is established by Hasselman including critical stress fracture theory and thermal shock damage theory [27,28]. Two parameters corresponding to the above theories could be specified: one is thermal stress fracture resistance parameter, R (describing the thermal shock resistance of brittle materials in terms of the maximum temperature increment within which the material can withstand without fracture), which can be expressed as [1,29]

$$R = \boldsymbol{\sigma}(1-v)/(E\boldsymbol{\alpha}). \quad (3)$$

The other is the thermal stress damage resistance parameter, R' (reflecting the resistance to catastrophic crack propagation of ceramics under a critical temperature difference), which can be expressed as [26,30]

$$R' = E\gamma/(\sigma^2(1-v)) \approx \left(K_{IC}/\boldsymbol{\sigma}\right)^2/(1-v), \quad (4)$$

where σ is the flexural strength, E is Young's modulus, α is the coefficient of thermal expansion, v is the Poisson ratio, γ is the fracture surface energy and K_{IC} is the fracture toughness.

According to Eqs. (3) and (4), the thermal shock resistance could be improved by the increase of K_{IC} and σ or the decrease of E and α [31]. In other words, to avoid thermal shock crack initiation a ceramic should possess a high flexural strength but a low coefficient of thermal expansion, Young's modulus, and Poisson's ratio. In contrast, a low flexural strength but a high Poisson's ratio, Young's modulus, and fracture energy would be desired for a ceramic to prevent thermal shock crack propagation [32]. Thus, the fact that the presence of ZrN particles led to an improvement of thermal shock resistance of AlON ceramic was attributed to the following possible reasons.

Firstly, the improved flexural strength and fracture toughness by the presence of nano-sized ZrN particles would play an important role in the improvement of thermal shock resistance of AlON ceramic. As Ma and Han [19] reported, the improvement in the fracture toughness and thermal shock resistance could be achieved by making composites in which the interfaces between the matrix and particles acted to deflect propagating cracks. Li et al. [33] also reported the mechanisms like crack branching and deflection that occurred at the interfaces between the two phases, impeding the crack growth. As reported in [17], the ZrN particles suppressed crack initiation and propagation, and changed the fracture mode from intergranular fracture for pure AlON ceramic to combination mode including intergranular and transgranular fracture. In the current study, it can also be seen from the fracture surfaces in Fig. 7(c) and (d) that the ZrN particles played a role in toughening AlON ceramic. Indeed, with or without thermal shock tests, the presence of nano-sized ZrN particles could alter the path of a crack impinging on a boundary, leading to crack deflection, crack bridging and crack branching (Fig. 7). Therefore, the presence of nano-sized ZrN particles would effectively increase both the flexural strength and fracture toughness. As a result, based on Eqs. (3) and (4) the ZrN particles improved the thermal shock resistance of AlON ceramic (Fig. 4).

Then, the difference in the thermal properties of the AlON and ZrN could have an effect on the thermal shock resistance of AlON materials, as indicated in Eq. (3). From the SEM fractographs (Fig. 7) and TEM micrographs of ZrN–AlON composites (Fig. 5), it could be found that the nano-sized ZrN particles were homogeneously distributed throughout the composites and located mainly at grain boundaries or triple junctions of AlON matrix. This would relax the interface stress caused by mismatched thermal expansion between AlON and ZrN during the abrupt thermal shock by pinning effect at the grain boundaries and provide favorable sites for the dissipation of energy associated with crack growth during fracture. Although the coefficient of thermal expansion (α) of ZrN is $6.0\times10^{-6}\,K^{-1}$ [34] that was a little higher than that of AlON (5.23×10^{-6}) [35], the coefficient of thermal conductivity of ZrN is $21.9\,W\,m^{-1}\,K^{-1}$ [12] that was remarkably higher than that of AlON ($10.3\,W\,m^{-1}\,K^{-1}$) [9]. Thus, the relatively high thermal conductivity of ZrN would bring about lower thermal stresses to facilitate the nucleation of microcracks during thermal shock tests. Reeves et al. [36] also reported that the thermal properties (i.e., thermal expansivity, thermal conductivity, and other properties associated with the use at high temperatures) were important in determining the thermal shock resistance of ceramic composites. Therefore, the improved thermal shock resistance of ZrN–AlON composites (Figs. 3 and 4) could be partly attributed to the superior thermal properties of the presence of ZrN particles.

Furthermore, the grain size and bulk density would also have an influence on the thermal shock resistance of AlON ceramic. You et al. [37] reported that the thermal shock resistance could be improved by decreasing grain size or increasing the bulk density. The thermal shock behavior of pure AlON ceramic with a relative density of 97% has been investigated in [10]. Indeed, as mentioned before, the presence of ZrN particles led to a refined AlON matrix grain size and a reduction of porosity. Thus, it would make a contribution to improvement of the thermal shock resistance of AlON ceramic.

In addition, it should be noted that, as shown in Figs. 3 and 4, Young's modulus of ZrN–AlON composites nonlinearly changed with increasing thermal shock temperature

or quenching/thermal shock times. Similar result was also reported in hot-pressed AlON-matrix composites reinforced with SiC particles [10]. It was reported that during the non-linear deformation Young's modulus of a material was a function of strain ε [2,10]. Then the magnitude of the thermal stress would be reduced for materials that exhibit non-linear elastic behavior, and the stress intensity factor or driving force for an unstable crack growth during thermal shock would also be decreased [2].

Based on these results and discussion, it can be concluded that the critical temperature difference of 2.7% ZrN–AlON composites for the abrupt degradation of flexural strength was 225 °C, which represented an increase of that by 12.5% in comparison with pure AlON ceramic. Consequently, the presence of nano-sized ZrN particles exhibited a positive effect on the improvement of the thermal shock resistance of the investigated AlON ceramic. However, more studies are needed to further improve and optimize the thermal shock resistance of AlON ceramic via varying amounts of nano-sized ZrN particles.

5. Conclusions

The thermal shock behaviors of 2.7% nano-sized ZrN particulate-reinforced aluminum oxynitride (AlON) composites were investigated by a water-quenching technique over a temperature range of 225 °C to 275 °C and the number of repeated quenchings up to 5 times at a constant temperature of 25 °C. Due to the presence of large temperature gradients and thermal stresses in the ZrN-AlON ceramic caused by the abrupt water-quenching, the residual flexural strength decreased gradually with increasing quenching temperature and thermal shock times. However, the decrease of Young's modulus with increasing temperature range and thermal shock times exhibited a non-linear behavior. The presence of nano-sized ZrN particles led to an increase in both of the residual strength and the critical temperature difference. This was mainly attributed to the toughening effects, the higher thermal conductivity of ZrN, the refined grain size and the reduction of porosity. A variety of toughening mechanisms in the ZrN nano-particulate reinforced AlON composites such as crack deflection, crack bridging and crack branching were observed during thermal shock experiments, hence increasing effectively the crack propagation resistance and resulting in a significant improvement in the flexural strength and fracture toughness of the composites.

Acknowledgments

The authors would like to thank the financial support of the National Natural Science Foundation of China (NSFC Grant nos. 51072121 and 50672060) and Natural Sciences and Engineering Research Council of Canada (NSERC) in the form of international research collaboration. D.L. Chen is also grateful for the financial support by NSERC-DAS Award, Premier's Research Excellence Award (PREA), Canada Foundation for Innovation (CFI), and Ryerson Research Chair (RRC) program. The authors would also like to thank Professor X.D. Sun (Northeastern University) for the helpful discussion and suggestion, and H.M. Kan (Shenyang University), Q. Li, A. Machin, J. Amankrah and R. Churaman (Ryerson University), for their assistance in the experiments. X.J. Zhao as an international exchange Ph.D. student also gratefully acknowledges the financial support provided by China Scholarship Council.

References

[1] N.M. Rendtorff, L.B. Garrido, E.F. Aglietti, Thermal shock resistance and fatigue of zircon–mullite composite materials, Ceramics International 37 (2011) 1427–1434.
[2] R.N. Singh, H.Y. Wang, Thermal shock behavior of fiber-reinforced ceramic matrix composites, Composites Engineering 5 (1995) 1287–1297.
[3] Y. Wang, J. Liang, W.B. Han, X.H. Zhang, Mechanical properties and thermal shock behavior of hot-pressed ZrB_2–SiC–AlN composites, Journal of Alloys and Compounds 475 (2009) 762–765.
[4] W.J. Li, Y. Zhang, X.H. Zhang, C.Q. Hong, W.B. Han, Thermal shock behavior of ZrB_2–SiC ultra-high temperature ceramics with addition of zirconia, Journal of Alloys and Compounds 478 (2009) 386–391.
[5] J. Podworny, J. Wojsa, T. Wala, Variation of Poisson's ratio of refractory materials with thermal shocks, Ceramics International 37 (2011) 2221–2227.
[6] P. Goeuriot, D. Goeuriot-Launay, F. Thevenot, Oxidation of an Al_2O_3–γAlON ceramic composite, Journal of Materials Science 25 (1990) 654–660.
[7] J. Zheng, B. Forslund, Carbothermal synthesis of aluminium oxynitride (AlON) powder: influence of starting materials and synthesis parameters, Journal of the European Ceramic Society 15 (1995) 1087–1100.
[8] X.J. Zhao, D.L. Chen, H.Q. Ru, N. Zhang, B. Liang, Oxidation behavior of nano-sized SiC particulate reinforced AlON composites, Journal of the European Ceramic Society 31 (2011) 2255–2265.
[9] N.D. Corbin, Aluminum oxynitride spinel: a review, Journal of the European Ceramic Society 5 (1989) 143–154.
[10] X.J. Zhao, H.Q. Ru, D.L. Chen, N. Zhang, B. Liang, Thermal shock behavior of nano-sized SiC particulate reinforced AlON composites, Materials Science and Engineering B 177 (2012) 402–410.
[11] D. Wu, Z. Zhang, W. Fu, X. Fan, H. Guo, Structure, electrical and chemical properties of zirconium nitride films deposited by dc reactive magnetron sputtering, Applied Physics A 64 (1997) 593–595.
[12] J. Adachi, K. Kurosaki, M. Uno, S. Yamanaka, Thermal and electrical properties of zirconium nitride, Journal of Alloys and Compounds 399 (2005) 242–244.
[13] B. Fu, L. Gao, Synthesis of nanocrystalline zirconium nitride powders by reduction–nitridation of zirconium oxide, Journal of the American Ceramic Society 87 (2004) 696–698.
[14] X.Y. Li, G.B. Li, F.J. Wang, T.C. Ma, D.Z. Yang, Investigation on properties of ceramic coatings of ZrN, Vacuum 43 (1992) 653–656.
[15] K. Schwarz, A.R. Williams, J.J. Cuomo, J.H.E. Harper, H.T.G. Hentzell, Zirconium nitride—a new material for Josephson junctions, Physical Review B 32 (1985) 8312–8316.
[16] X.J. Zhao, N. Zhang, H.Q. Ru, B. Liang, D.L. Chen, Mechanical properties and toughening mechanisms of silicon carbide nano-particulate reinforced AlON composites, Materials Science and Engineering: A 538 (2012) 118–124.
[17] X.J. Zhao, D.L. Chen, H.Q. Ru, N. Zhang, Zirconium nitride nano-particulate reinforced AlON composites: fabrication, mechanical properties and toughening mechanisms, Journal of the European Ceramic Society 31 (2011) 883–892.

[18] M. Hamidouche, N. Bouaouadja, C. Olagnon, G. Fantozzi, Thermal shock behavior of mullite ceramic, Ceramics International 29 (2003) 599–609.
[19] B.X. Ma, W.B. Han, Thermal shock resistance of ZrC matrix ceramics, International Journal of Refractory Metals and Hard Materials 28 (2010) 187–190.
[20] J.K. Chen, K.L. Tang, J.T. Chang, Effects of zinc oxide on thermal shock behavior of zinc sulfide–silicon dioxide ceramics, Ceramics International 35 (2009) 2999–3004.
[21] K. Chang, W.M. Feng, L.Q. Chen, Effect of second-phase particle morphology on grain growth kinetics, Acta Materialia 57 (2009) 5229–5236.
[22] Y.W. Bao, X.H. Wang, H.B. Zhang, Y.C. Zhou, Thermal shock behavior of Ti_3AlC_2 between 200 °C and 1300 °C, Journal of the European Ceramic Society 25 (2005) 3367–3374.
[23] N. Noda, L.C. Guo, Thermal shock analysis for a functionally graded plate with a surface crack, Acta Mechanica 195 (2008) 157–166.
[24] G.D. Quinn, N.D. Corbin, J.W. McCauley, Thermomechanical properties of aluminum oxynitride spinel, American Ceramic Society Bulletin 63 (1984) 723–730.
[25] J.C. Han, B.L. Wang, Thermal shock resistance of ceramics with temperature-dependent material properties at elevated temperature, Acta Materialia 59 (2011) 1373–1382.
[26] A.A. Buchheit, G.E. Hilmas, W.G. Fahrenholtz, D.M. Deason, Thermal shock resistance of an AlN–BN–SiC ceramic, Journal of the American Ceramic Society 92 (2009) 1358–1361.
[27] C.Y. Tian, N. Liu, M.H. Lu, Thermal shock and thermal fatigue behavior of Si_3N_4–TiC nano-composites, International Journal of Refractory Metals and Hard Materials 26 (2008) 478–484.
[28] D.P.H. Hasselman, Unified theory of thermal shock fracture initiation and crack propagation in brittle ceramics, Journal of the American Ceramic Society 52 (1969) 600–604.
[29] A.A. Buchheit, G.E. Hilmas, W.G. Fahrenholtz, D.M. Deason, H. Wang, Mechanical and thermal properties of AlN–BN–SiC ceramics, Materials Science and Engineering: A 494 (2008) 239–246.
[30] D.Y. Li, H. Yang, G.J. Qiao, Z.H. Jin, Study on thermal shock behavior of SiC/BN laminated ceramics composites, Journal of Materials Science and Engineering 24 (2006) 17–19.
[31] A. Kovalcikova, J. Dusza, P. Sajgalik, Thermal shock resistance and fracture toughness of liquid-phase-sintered SiC-based ceramics, Journal of the European Ceramic Society 29 (2009) 2387–2394.
[32] J.H. She, J.F. Yang, T. Ohji, Thermal shock resistance of porous silicon nitride ceramics, Journal of Materials Science Letters 22 (2003) 331–333.
[33] Z.Q. Li, J.C. Liu, H.Y. Du, S. Li, P.Y. Zhang, Thermal shock resistance of dense zirconia matrix composites evaluated by indentation techniques, Materials Science and Engineering: A 517 (2009) 154–159.
[34] M. Ishitsuka, T. Sato, T. Endo, M. Shimada, Thermal shock fracture behavior of ZrO_2 based ceramics, Journal of Materials Science Letters 24 (1989) 4057–4061.
[35] E.K. Graham, M.C. Munly, J.W. McCauley, N.D. Corbin, The elastic properties of polycrystalline aluminum oxynitride spinel (ALON) and their dependence of pressure, temperature and composition, Journal of the American Ceramic Society 71 (1988) 807–812.
[36] A.J. Reeves, R. Taylor, T.W. Clyne, The effect of interfacial reaction on thermal properties of titanium reinforced with particulate SiC, Materials Science and Engineering: A 141 (1991) 129–138.
[37] X.Q. You, T.Z. Si, N. Liu, P.P. Ren, Y.D. Xu, J.P. Feng, Effect of grain size on thermal shock resistance of Al_2O_3–TiC ceramics, Ceramics International 31 (2005) 33–38.